Technical Note
radphi-2003-701

# LGD shower resolution

Mihajlo Kornicer
Richard T. Jones
University of Connecticut, Storrs, CT

July 28, 2003

**Abstract**

The energy and spatial resolution in the LGD are measured using 2-shower invariant mass distributions from $\eta \to 2\gamma$ and $\pi^0 \to 2\gamma$ decays. The mass resolution of the $\eta$ is mainly driven by the shower energy resolution while the width of the $\pi^0$ has a large spatial resolution contribution. Simultaneous analysis of the $\eta$ and $\pi^0$ data enables extraction of the parameters that describe both the shower energy and spatial resolution of the LGD.

# 1 Introduction

The invariant mass resolution of mesons that undergo $2\gamma$ decay is determined by the single shower energy and position resolutions. In the case where spatial contribution can be neglected, one can extract the single shower energy resolution by measuring the invariant mass resolution in narrow energy bins. The spatial contribution is expected to be small when the two showers are well separated. In the case where two showers are closer in space, shower centroid resolution can have a larger impact on the mass resolution.

Assuming that the spatial resolution is not important for $\eta(2\gamma)$ decays, we extracted the shower energy resolution function without assuming any functional form. This model-independent solution is then compared with the standard parametrization of the lead glass energy resolution. In order to describe the $\pi^0$ mass with the same parameters, one has to take the spatial resolution into account. We introduced one additional parameter that scales the spatial contribution to the mass resolution. All parameters have been determined by simultaneous analysis of the $\eta$ and $\pi^0$ data.

# 2 The invariant mass resolution

The square of the invariant mass of two photons is given by

$$M^2 = 4E_1E_2\sin^2\frac{\theta_{12}}{2} = 2E_1E_2(1-\cos\theta_{12}), \tag{1}$$

where $E_1$ and $E_2$ are corresponding photon energies, while $\theta_{12}$ is their angular separation. The expression for the variance of the squared invariant mass in terms of the variances of energy and shower position in the LGD is given by

$$V(M^2) = \sum_{i=1}^{2}\left[\left(\frac{\partial M^2}{\partial E_i}\right)^2 V_E + \left(\frac{\partial M^2}{\partial x_i}\right)^2 V_X + \left(\frac{\partial M^2}{\partial y_i}\right)^2 V_Y + 2\left(\frac{\partial M^2}{\partial x_i}\right)\left(\frac{\partial M^2}{\partial y_i}\right)V_{XY}\right], \tag{2}$$

where index $i$ counts photons. Taking all derivatives of Eq. (1) one can re-write Eq. (2) in the form

$$\frac{V(M^2)}{M^4} = \frac{V_E(E_1)}{E_1^2} + \frac{V_E(E_2)}{E_2^2} + \frac{V_S(M^2)}{M^4}, \tag{3}$$

where spatial derivatives and variances are grouped into the term $V_S(M^2)$. The usual expression for the energy resolution function is given by [1]

$$\frac{\sigma_E}{E} = \sqrt{\frac{V_E}{E^2}} = A + \frac{B}{\sqrt{E}}, \tag{4}$$

where parameters $A$ and $B$ have to be determined. Spatial derivatives can be expressed in terms of measured photon momenta utilizing the expression

$$\cos(\theta_{12}) = \frac{\vec{P_1}\cdot\vec{P_2}}{\left|\vec{P_1}\right|\left|\vec{P_2}\right|} = \frac{x_1x_2+y_1y_2+z_1z_2}{\sqrt{x_1^2+y_1^2+z_1^2}\sqrt{x_2^2+y_2^2+z_2^2}}. \tag{5}$$

For example

$$\frac{\partial M^2}{\partial x_1} = -2E_1E_2\frac{\partial\cos(\theta_{12})}{\partial x_1} = -\frac{2P_{z_1}}{z_0E_1^2}\left[P_{x_2}(P_{y_1}^2+P_{z_1}^2) - P_{x_1}(P_{y_1}P_{y_2}+P_{z_1}P_{z_2})\right]. \tag{6}$$

The other spatial derivatives have a similar form and they can be obtained by the proper variable substitution. The $z$ position of the shower maximum is not directly measured. However, it is correlated with the energy and this has been taken into account within the shower-depth and nonlinearity corrections [2]. For the purpose of this analysis a common $z$-plane is fixed at $z_0 = 120\ cm$. The fluctuations in the shower position that determine $V_X$, $V_Y$ and $V_{XY}$ are also affected by the energy. The energy dependence is proportional to $1/\sqrt{E}$ with a proportionality constant that depends on the size of the LGD block [3]. This term alone would make spatial errors cylindrical and uniform across the face of the LGD. However, one can expect that the uncertainty in the shower position increases with polar angle $\theta$, as $X_0\cos\theta$, where $X_0$ is the radiation length

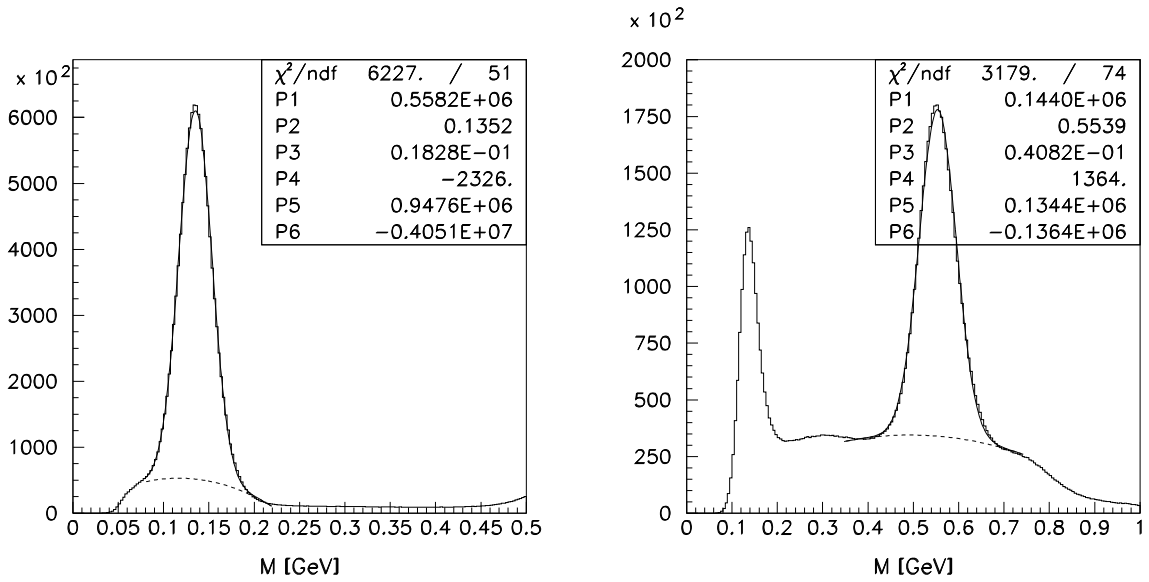


Figure 1: Invariant mass distribution of $\pi^0(2\gamma)$ (left) and $\eta(2\gamma)$ (right).

of the lead glass. This makes shower centroid errors elliptical. The orientation of the ellipse depends on the shower azimuthal angle $\phi$, and is connected with the correlation term $V_{XY}$. Combining all together,

$$\begin{aligned} V_X &= \sigma_x^2 = \frac{C_E^2}{E} + \left(X_0 \sin\theta \cos\phi\right)^2, \\ V_Y &= \sigma_y^2 = \frac{C_E^2}{E} + \left(X_0 \sin\theta \sin\phi\right)^2, \\ V_{XY} &= X_0^2 \sin^2\theta \cos\phi \sin\phi, \end{aligned} \tag{7}$$

with $C_E = 7.1$ mm$\cdot$GeV$^{\frac{1}{2}}$, and $X_0 = 31.6$ mm[4].

In this study, we analyze events with two reconstructed showers. The $\pi^0$ sample, consisting of $15M$ events, is selected by limiting invariant mass to $M < 0.5\ GeV$. The corresponding invariant mass distribution is shown on the left side of Fig. 1. The $\eta$ sample is obtained by selecting pairs with shower separation $D_{\gamma\gamma} \geq 20\ cm$. This distance is approximately twice the average shower size in the LGD plane. The corresponding $\eta$ mass distribution, shown on the right side of Fig. 1, contains $8M$ events. Small peak around $0.2\ GeV$ represents the $\pi^0$ remnants that have large shower separation. The $\pi^0$ and $\eta$ peaks are fitted with a Gaussian over a polynomial background. In order to check the influence of spatial resolution on the overall mass resolution, the distribution of $V_s(M^2)/M^4$ is plotted in Fig. 2 (solid line), calculated with the help of Eqs. (6) and (7). The distribution is obtained from the inclusive $2\gamma$ sample without restrictions on $M$ or $D_{\gamma\gamma}$. The dotted and dashed lines represent pairs with invariant mass within a $2\sigma$ window around the $\pi^0$ and $\eta$ peaks, respectively. Table 1 shows the Gaussian mean and *r.m.s.* of the two fitted meson peaks from Fig. 1. The third column represents the $V(M^2)/M^4$ obtained from the fit. (see Eq. (8)). The last column represents the mean value of $V_s(M^2)/M^4$ from the dashed and dotted distributions in Fig 2. One can see that the spatial resolution contributes about 10% to the $\eta$ variance, while the $\pi^0$ width is affected at the level of 50%.

When two showers have the same energies and the spatial term is small, Eq. (3) is reduced to

$$\frac{V(M^2)}{M^4} = 4\frac{V(M)}{M^2} = 2\frac{V_E}{E^2}. \tag{8}$$

By measuring the mass or squared mass resolution in narrow energy bins one can extract the energy resolution function Eq. (4) and the corresponding parameters. The energy bins should be narrower than the detector energy resolution.

Table 1: The mean, *r.m.s.* and corresponding $V(M^2)/M^4$ obtained from the fit of the two meson peaks in Fig. 1. The last column is the mean of dashed and dotted distributions from Fig 2, respectively.

| Data | $\mu\ [GeV]$ | $\sigma\ [GeV]$ | $V(M^2)/M^4$ | $V_s(M^2)/M^4$ |
|---|---|---|---|---|
| $\pi^0$ | 0.1352 | 0.0183 | 0.0731 | 0.0406 |
| $\eta$ | 0.5539 | 0.0408 | 0.0217 | 0.0030 |

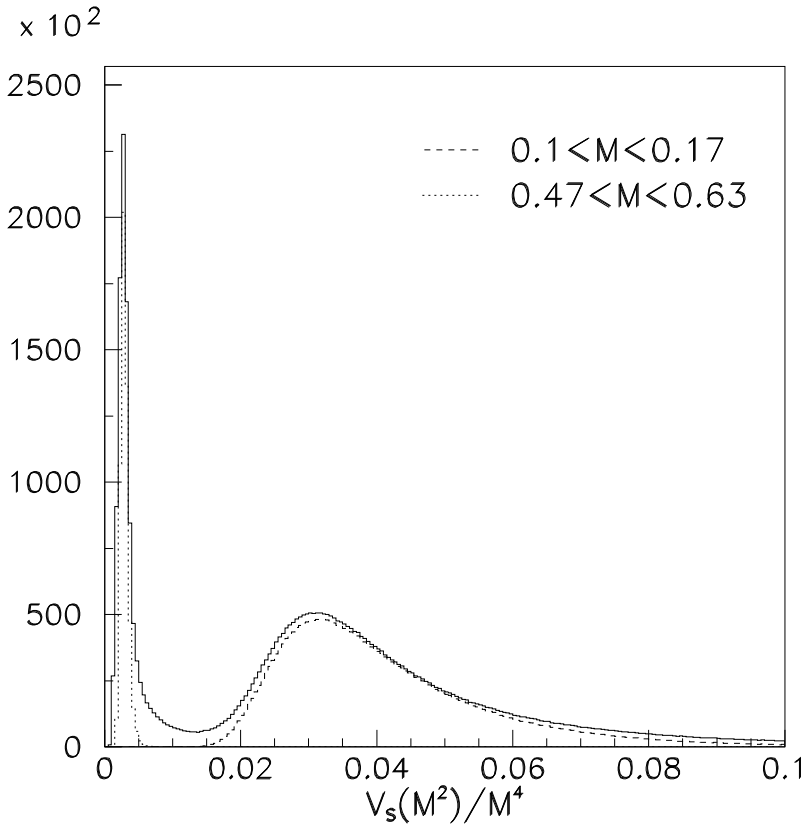


Figure 2: The $V_S(M^2)/M^2$ distribution in $2\gamma$ events calculated using Eqs. (6) and (7). The dashed and dotted lines represent the distribution for pairs with mass within the $\pi^0$ and $\eta$ windows, respectively.

# 3 The energy resolution

Fig. 3 shows the energy distribution of the harder shower ($E_1$) vs. the softer shower ($E_2$) for the $2\gamma$ samples. Showers with separation $D_{\gamma\gamma} \geq 20\ cm$ are shown on the left, while pairs with $M < 0.5\ GeV$ are plotted on the right of Fig. 3. Green dots represent the pairs with masses inside the respective meson window. Solid lines represent the case where $E_1 = E_2$. Fig. 3 shows that the statistics of pairs with $E_1 = E_2$ is quite poor and covers a restricted energy range. Consequently, we measured $V(M^2)$ for the set of $(E_1, E_2)$ values shown as black dots in Fig. 3. For each dot, the squared mass distribution ($\eta$ sample) or the invariant mass distribution ($\pi^0$ data) has been created. Energy limits for a dot have been chosen to be the $0.5\sigma_E$ for each $E$, where $\sigma_E$ is deduced from Eq. (4) with $A = 0.02$ and $B = 0.08$ Gev$^{\frac{1}{2}}$. These distributions, shown in Figs. 4 - 7, are all fitted with a Gaussian over a polynomial background. Fitting errors reflect the statistics of the data sample. Systematic errors are governed by the choice of background function, and they are estimated to be 5% and 10% for the $\eta$ and $\pi^0$ data respectively. Reducing the energy bins to $0.3\sigma_E$ did not have a significant impact on the results; it only reduced statistics. From the Gaussian fit the value $V(M^2)/M^4$ has been calculated.

In the first approximation, for the $\eta$ data we neglected the spatial contribution to the mass resolution. Following Eq. (3) we formed the set of equations

$$\left(\frac{V(M^2)}{M^4}\right)_k = F_i + F_j, \tag{9}$$

where $k = 1, \ldots, 18$ labels calculated values. We try to solve these equations for the set of $F_i$ values, with $i = 1, \ldots, 11$ numbering the selected photon energies. The least-square solution we obtained is model-independent since we have not presumed the functional form of $F(E)$. It is free of any restrictions on the $F$ values except that $F_i = F_j$ for $i = j$. The corresponding $\sigma_E(E_i) = E_i\sqrt{F_i}$ from the free solution is plotted in Fig. 8. These points agree very well with the standard expression for the energy resolution (Eq. 4), with $A = 0.037$ and $B = 0.080$ GeV$^{\frac{1}{2}}$.

# 4 Spatial corrections

In order to include the spatial corrections to the mass resolution we recorded the mean of the $V_s(M^2)/M^4$ distributions for each $(E_1, E_2)$ bin for both the $\eta$ and $\pi^0$ samples. Then we modified the expression for the variance function (Eq. (3)), using Eq. (4) for the contribution from energy resolution,

$$\frac{V(M^2)}{M^4} = \left(A + \frac{B}{\sqrt{E_1}}\right)^2 + \left(A + \frac{B}{\sqrt{E_2}}\right)^2 + C\frac{V_s(M^2)}{M^4}. \tag{10}$$

In addition to the standard parameters $A$ and $B$, we introduced parameter $C$ that scales the spatial resolution contribution. With this simple model we first fitted $\eta$ data with $C$ set to zero. The fit is shown as the solid line in Fig. 8, while the fit parameters are shown in the first row of Table 2. Next we let $C$ vary. The corresponding fit is represented by the dashed line in Fig. 8 and the second row in Table 2. The fit confirms that the $\eta$ mass is not very sensitive to spatial corrections. In the next step we fitted all measured points from the $\eta$ and $\pi^0$ samples together. The fit is shown as the dotted line in Fig. 8, and the resulting parameters are shown in the last row of Table 2. Both the $\pi^0$ and $\eta$ mass distributions are described well by the model.

We used a single parameter to scale the spatial contribution to the mass resolution. The energy-dependent part of the spatial error in Eq. (7) is dominant at small and moderate angles $\theta \approx 10\,$deg, while the angular part in Eq. (7) becomes more important at large angles $\theta > 15\,$deg. We checked the importance of the angle-dependent spatial errors by setting $X_0 = 0$ in Eq. (7), which made the overall $\chi^2$ worse. We conclude that it is important to use elliptically errors at larger angles. The scale parameter $C$ can be viewed as a correction to the nominal value of $C_E = 7.1$ mm$\cdot$GeV$^{\frac{1}{2}}$ for the LGD.

# 5 Conclusion

We analyzed the invariant mass distributions from $\pi^0 \to 2\gamma$ and $\eta \to 2\gamma$ decays to extract the single shower energy and position resolution. To a good approximation, the width of the $\eta$ mass peak is mainly determined by the energy resolution, while the $\pi^0$ mass is heavily affected by the spatial resolution. This feature is related

Table 2: The parameter values from different fits to the $\eta$ and $\pi^0$ mass resolutions, obtained using Eq. (10). The corresponding fits are shown in Fig. 8

| Fit | $A$ | $B$ $\left[GeV^{-1/2}\right]$ | $C$ | $\chi^2$ |
|---|---|---|---|---|
| $\eta$ $(C=0)$ | $0.0371 \pm 0.0006$ | $0.0797 \pm 0.0008$ | 0 | 1.05 |
| $\eta$ (full) | $0.036 \pm 0.008$ | $0.080 \pm 0.003$ | $0.26 \pm 1.76$ | 1.04 |
| $\eta + \pi^0$ (full) | $0.035 \pm 0.004$ | $0.073 \pm 0.006$ | $0.90 \pm 0.02$ | 1.50 |

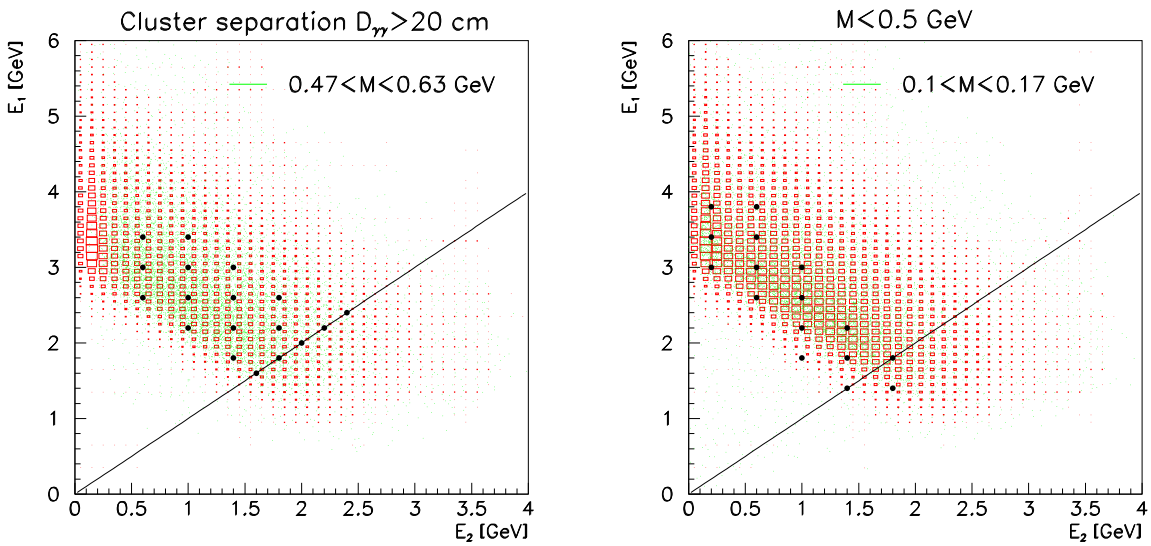


Figure 3: Energy distribution of $E_1$ vs. $E_2$ (red boxes). Green dots represent showers with invariant mass close to the $\pi^0$ mass (right) and $\eta$ mass (left). Black dots represent the pairs of photon energies for which $V(M^2)$ has been fitted. Solid lines correspond to the case when $E_1 = E_2$.

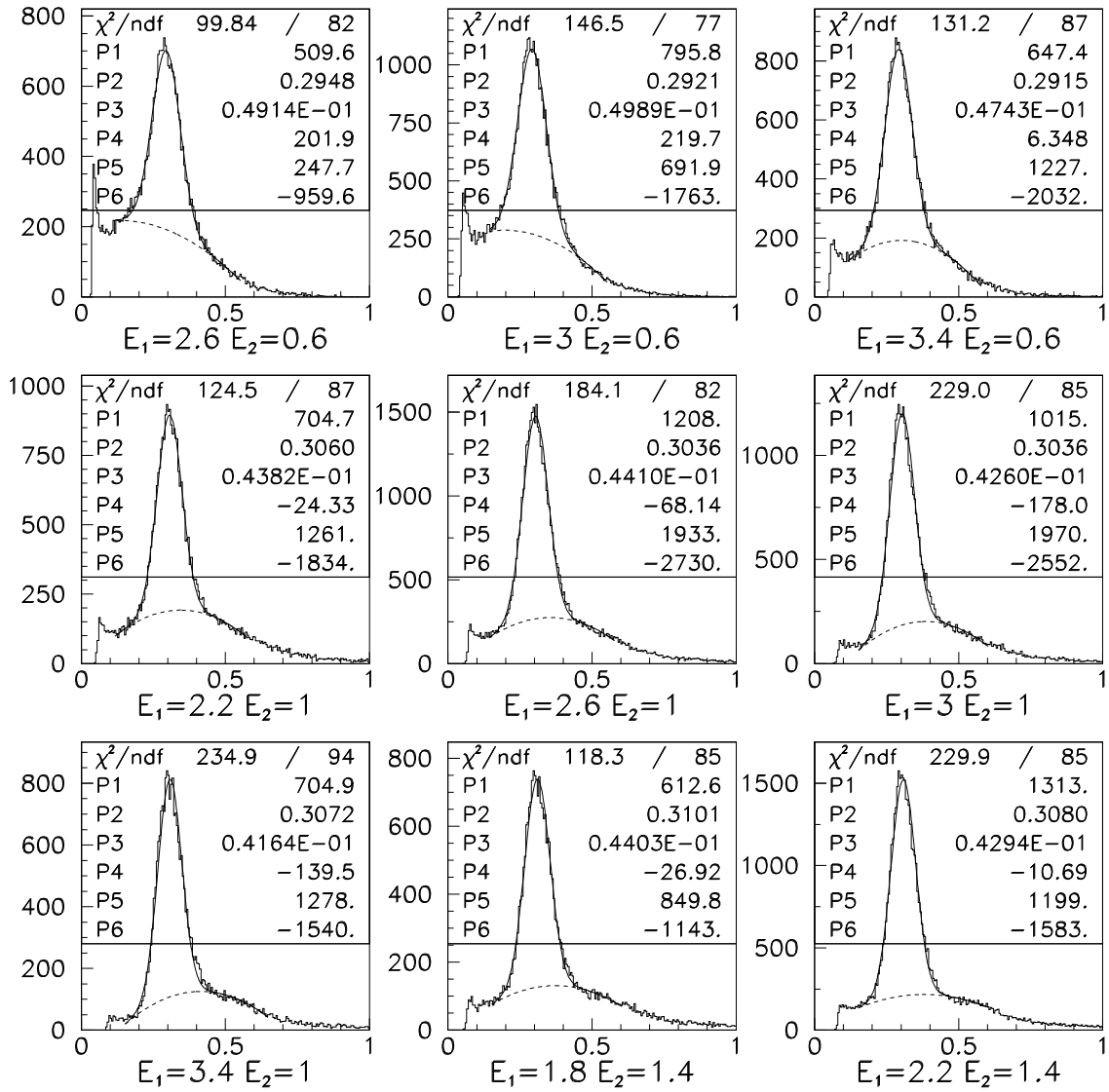


Figure 4: The $\eta$ squared-mass distributions for 9 energy bins, fitted with a Gaussian. The dotted lines represent a polynomial background. Below each plot are shown the corresponding energies $(E_1, E_2)$.

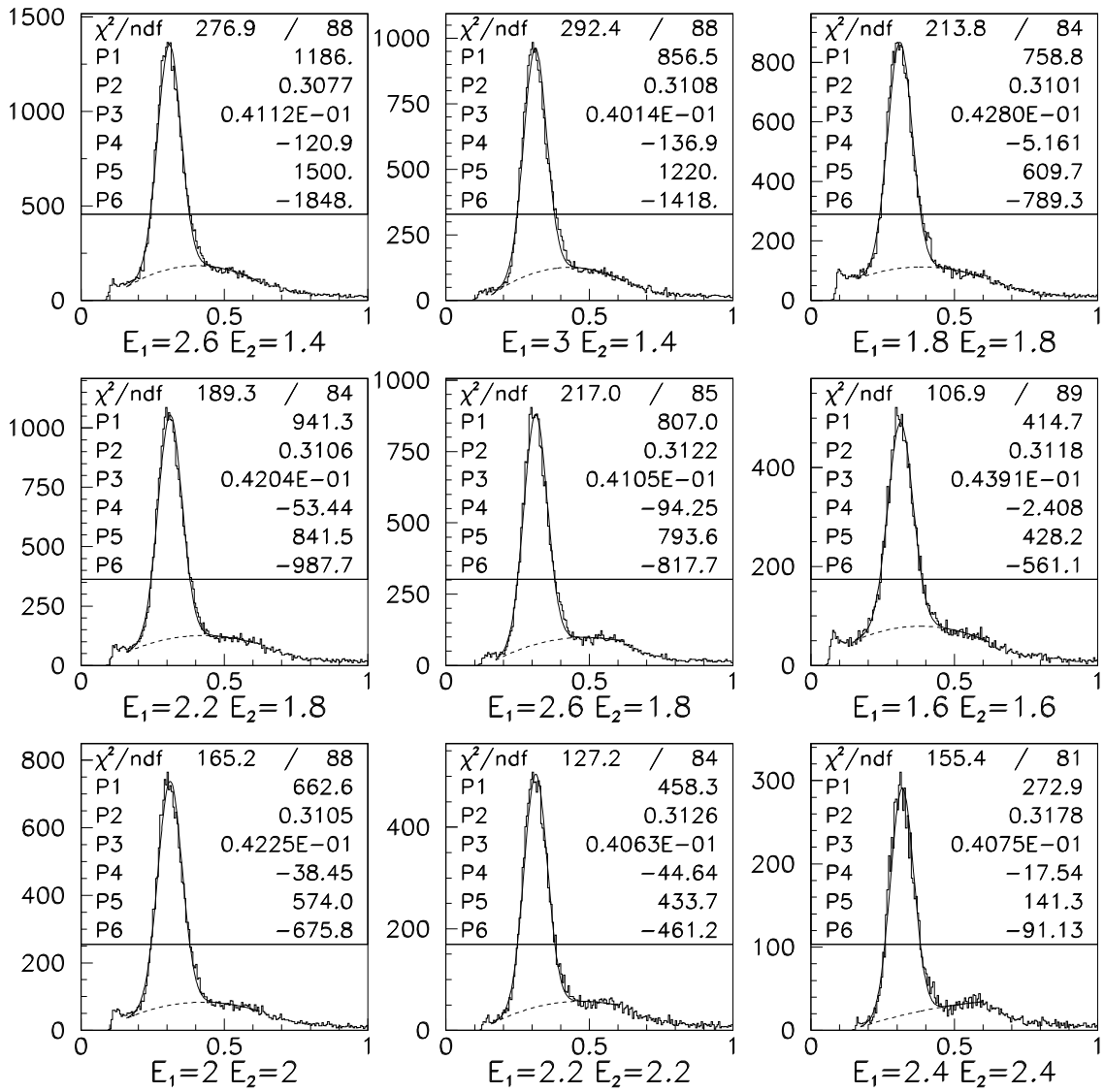


Figure 5: The same as Fig. 4 for energy bins $10 - 18$.

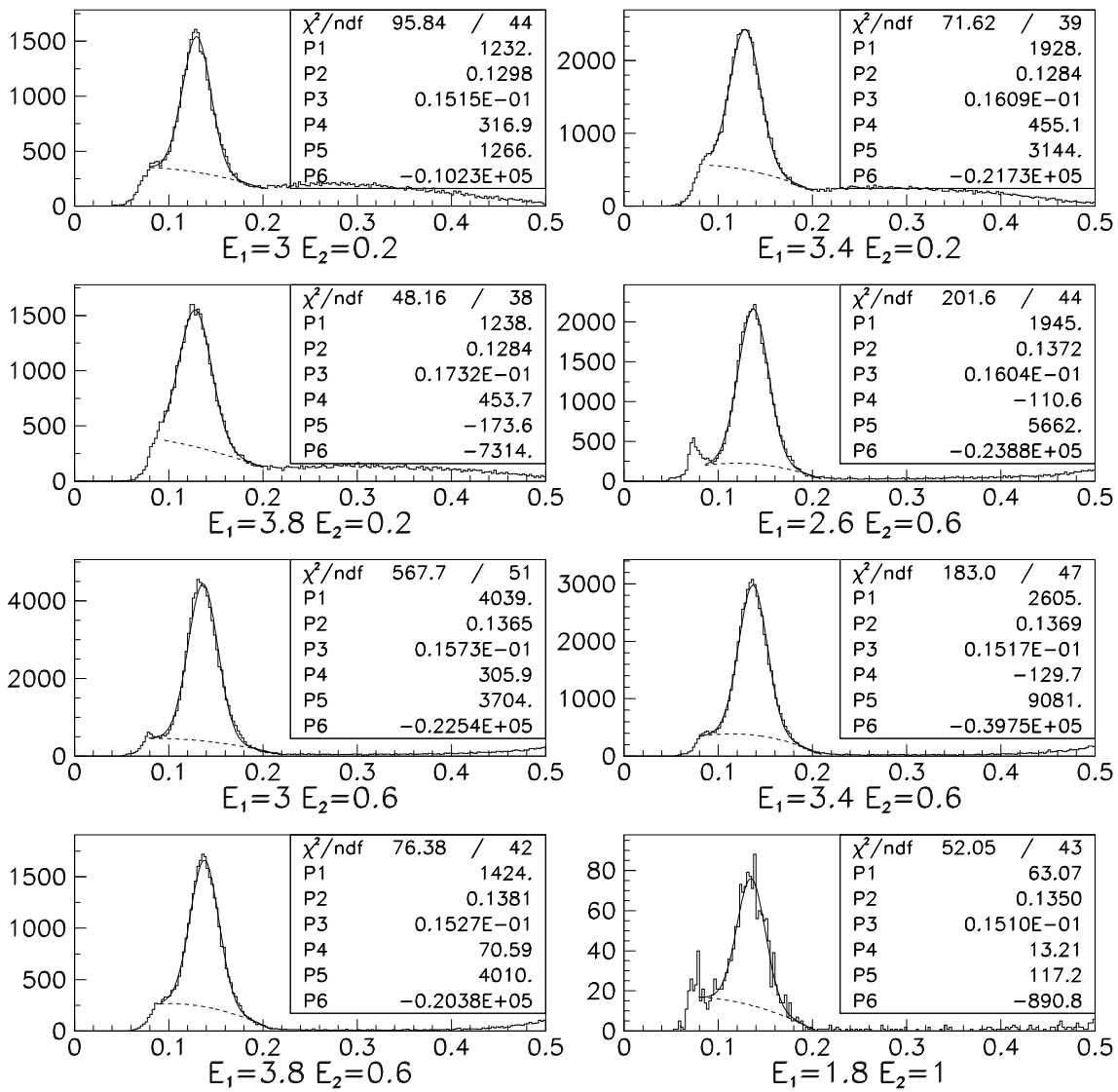


Figure 6: The $\pi^0$ mass distribution for 8 energy bins, fitted with a Gaussian. The dotted lines represent a polynomial background.

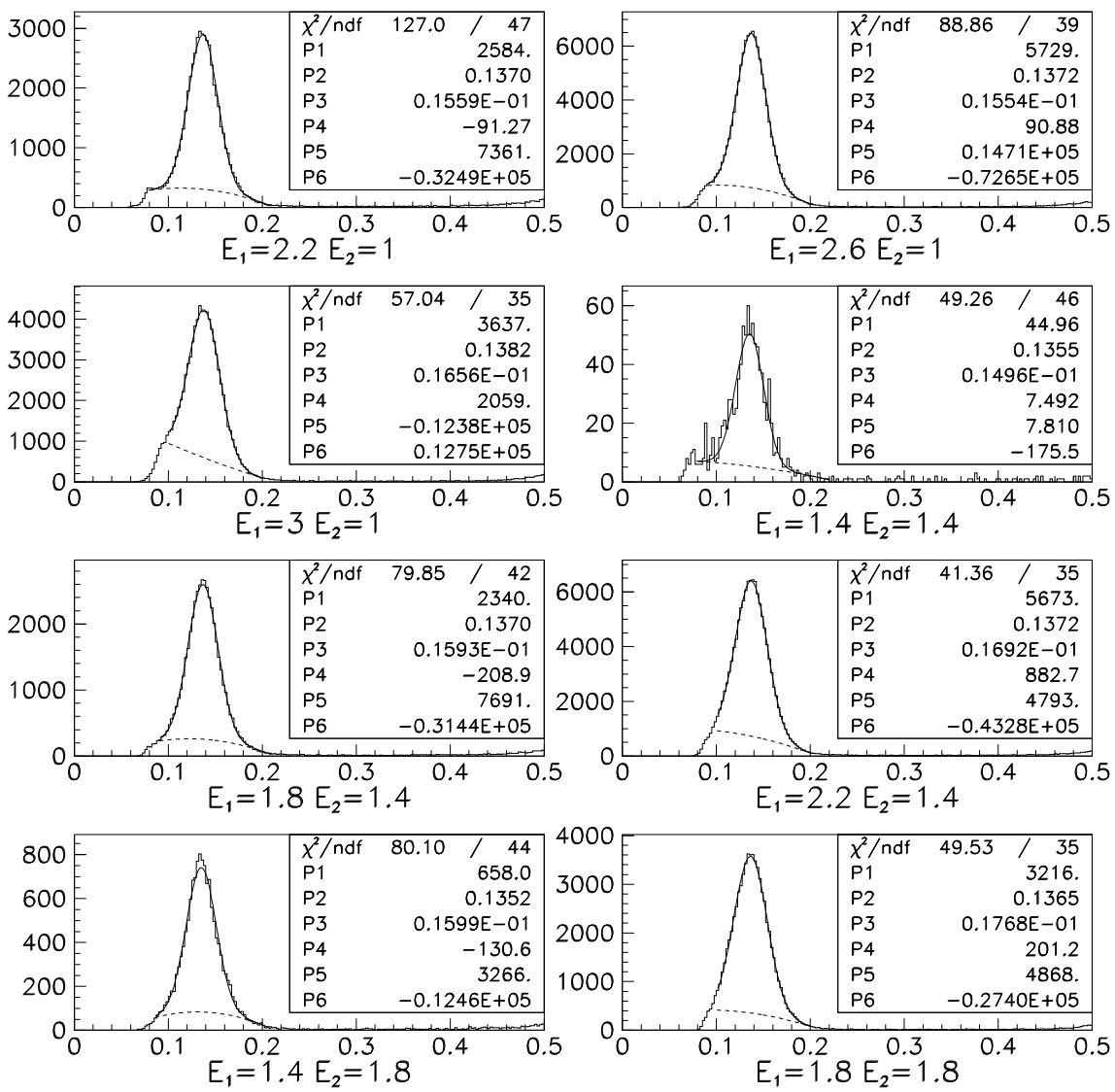


Figure 7: The same as Fig. 6 for energy bins $9-16$.

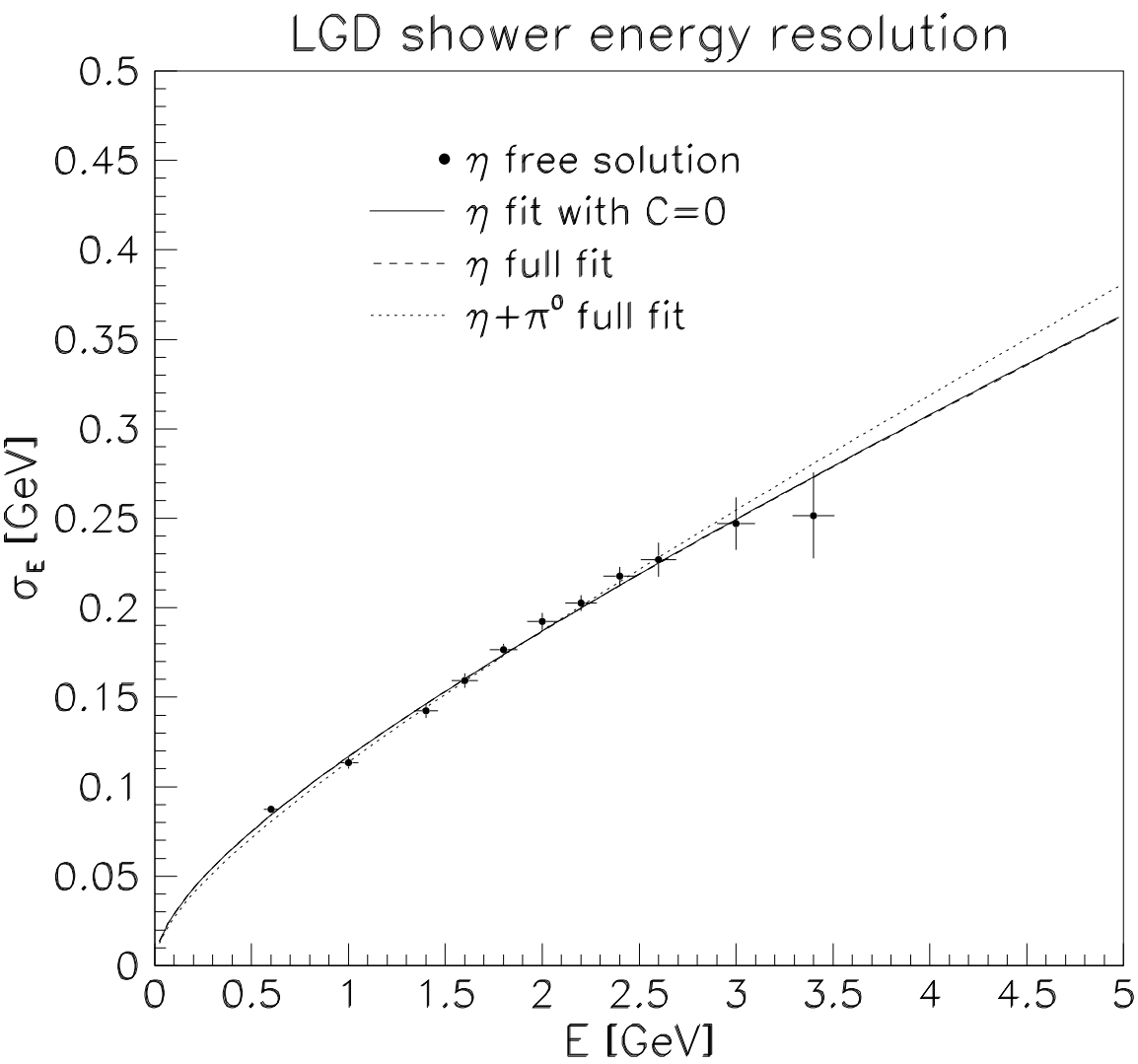


Figure 8: Energy resolution of showers in the LGD obtained from analysis of the $2\gamma$ sample. Points represent the free solution to the $\eta$ squared-mass resolution measurements when the contribution from the spatial resolution has been neglected. The solid line represents the fit to the $\eta$ data with the standard energy resolution model (Eq. (10)with $C = 0$). The dashed line represents the fit to the $\eta$ data when the spatial contribution is taken into account by Eq. (10). The dotted line corresponds to the simultaneous fit to the $\eta$ and $\pi^0$ data with the same function (Eq. (10)). Corresponding fit parameters and $\chi^2$ are shown in Table 2.

to the fact that the detector is close to the target and $\pi^0$ shower pairs from have separations close to the detector acceptance.

In the first approximation we neglected the spatial contribution to the $\eta$ mass resolution and measured the squared-mass variance for a set of well-defined shower energies $(E_1, E_2)$. From this measurement we a obtained model-independent solution to the energy resolution function. This solution is in good agreement with the standard expression used to describe the energy resolution of lead glass. In order to incorporate the $\pi^0$ data into the same description, we introduced a standard expression for the shower centroid resolution. The spatial contribution to the mass resolution is scaled by a free parameter $C$. The $\eta$ data showed no sensitivity to the value of the parameter $C$. In order to fix the set of parameters that governs the LGD resolution, we performed a simultaneous fit to 34 $\eta$ and $\pi^0$ mass resolution measurements. From the fit, we obtained for the energy resolution function

$$\frac{\sigma_E}{E} = 3.6\% + \frac{7.3\%}{\sqrt{E}},$$

and for the shower position uncertainty

$$\sigma_\rho = \sqrt{\left(\frac{0.64}{\sqrt{E}}\right)^2 + (X_0 \sin\theta)^2}, \quad \rho\sigma_\phi = \frac{0.64}{\sqrt{E}},$$

where $(\rho, \phi)$ are the polar coordinates of the shower in the face of the LGD. All lengths in these relations are in mm and all energies in GeV. The mass widths of both the $\pi^0$ and $\eta$ from $2\gamma$ events are explained very well with this single set of parameters.

# References


[1] "Data Analysis Techniques for High-Energy Physics", R. Frühwirth, M. Regler, R. K. Bock, H. Grote, D. Notz, Cambridge University Press 2000.

[2] "Energy nonlinearity and depth correction of showers in the LGD ", R.T Jones, Radphi TechNote *2002-201* (February 2001).

[3] "Calorimetry: Energy Measurements in Particle Physics", R. Wingman, International Series of Monographs on Physics 107, Oxford University Press (2000).

[4] C. P. Steffen, Ph.D. thesis, Indiana University (October 2001).